Experiments on Structure of Laser-Driven Detonations

Takuma Endo[1], Naohito Suwa[1], Tomohisa Honda[1], Shiro Taki[1], Hiroyuki Shiraga[2], Keisuke Shigemori[2], Mayuko Koga[2]

[1]Department of Mechanical Engineering, Hiroshima University
Higashi-Hiroshima, 739-8527, Japan

[2]Institute of Laser Engineering, Osaka University
Suita, 565-0871, Japan

1 Introduction

Detonation is originally a term in the field of chemical combustion [1]. However, two other types of detonation are now known: laser-driven (LD) detonation [2] and nuclear-combustion-driven (NCD) detonation [3, 4]. The common feature of detonation is that a shock wave and a fluid-heating zone propagate together interactively. A detonation speed is given by the Chapman-Jouguet condition as

$$D_{\mathrm{CJ}} = \sqrt{2\left(\gamma_{\mathrm{CJ}}{}^2 - 1\right)\left(q_{\mathrm{react}} + q_{\mathrm{ext}}\right)} \qquad (1)$$

where γ_{CJ}, q_{react}, q_{ext} are the specific-heat ratio at the rear surface, the heat of reaction per unit mass, and the added heat from external energy source per unit mass respectively. In chemical-combustion-driven (CCD) and NCD detonations, $q_{\mathrm{react}} > 0, q_{\mathrm{ext}} = 0$. However, $q_{\mathrm{react}} < 0, q_{\mathrm{ext}} > 0$ in LD detonations.

Although CCD detonations have been studied extensively, details of LD and NCD detonations have hardly been known. They are different from CCD detonations in the way that they contain hot plasma. Because energetic particles with long mean free path are produced in the plasma, the characteristics of LD and NCD detonations can be governed by their transport. Hence, studies of LD detonations by laboratory experiments can contribute to the field of inertial confinement fusion [3] and/or supernova explosion [4], which are relevant to NCD detonations.

Figure 1 shows an LD detonation. Laser starts to be absorbed in leading-shock-produced plasma by inverse bremsstrahlung. By the laser heating, ionization proceeds downstream. Because laser-absorption coefficient per unit length κ is scaled as

$$\kappa \propto \frac{z^2 n_{\mathrm{e}} n_{\mathrm{i}}}{T_{\mathrm{e}}^{3/2}\sqrt{1-\left(n_{\mathrm{e}}/n_{\mathrm{cr}}\right)}} \qquad (2)$$

where $z, n_{\mathrm{e}}, n_{\mathrm{i}}, T_{\mathrm{e}}, n_{\mathrm{cr}}$ are ionic charge state, electron density, ion density, electron temperature, and critical electron density for the laser respectively,

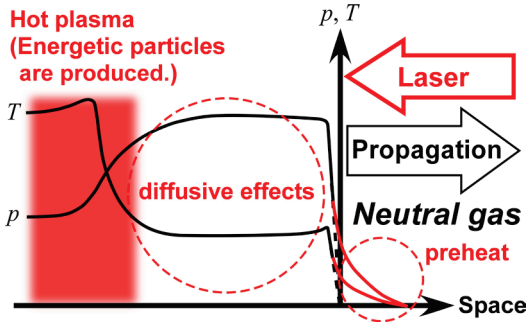

Figure 1. Schematic of laser-driven detonation.

Correspondence to: takumaendo@hiroshima-u.ac.jp

the laser heating becomes more remarkable nonlinearly as the ionization proceeds. This is a simplified description of an LD detonation. In this paper, we present experimental results on quasi-planar LD detonations where self-emission and Schlieren images of the detonations were observed edge-on.

2 Experimental arrangement

Experiments were carried out using GEKKO XII-HIPER laser system [5] at ILE, Osaka University. Figure 2 shows the experimental arrangement. A planar aluminum target was irradiated by laser in nitrogen gas at room temperature for creating a seed plasma for LD-detonation initiation. The pulse shape of the drive laser is shown in Fig. 2. The spot diameter of the laser irradiation d_{spot} was 1.3-2.5 mm. The energy flux of the drive laser S_L was $0.1\text{-}2.3\times10^{10}$ W/cm^2. For diagnostics, self-emission and Schlieren images were observed by a streak camera (SC) and a gate camera (GC) respectively. The lens L1 was the objective lens, which was an achromatic lens of 500 mm in focal length and 25 mm in effective diameter. The center axis of the drive laser was observed by the SC. By dividing the optical path to the GC into two and making their path lengths different, two gated images at different times were simultaneously observed. The exposure duration of the GC was 200 ps.

3 Results and discussions

Typical data are shown in Figs. 3-5, where p_1 is the initial gas pressure. A streaked self-emission image shows that a hot region propagated from left to right with an almost constant speed. The origin of the coordinate y corresponds to the height of the center axis of the drive laser, and that of x corresponds to the initial target position at $y=0$. The timings of the gated images are shown in the corresponding streaked image. Because the detonations propagated in gas, the peripheral borders of the fronts were affected by rarefaction waves, and the shape of the shock waves became a truncated cone. However, the central portions of the fronts were fairly planar.

The Schlieren images were created by probe-laser refraction due not only to the gradient of mass density $\partial\rho/\partial x$ but also to that of free-electron density $\partial n_e/\partial x$. In the optical arrangement shown in Fig. 2, the Schlieren image becomes dark when $\partial\rho/\partial x<0$, and it becomes bright when $\partial n_e/\partial x<0$. Therefore, a truncated-cone-shaped shock wave propagating from left to right makes a trapezoidal dark Schlieren image. As another feature of the presented Schlieren images, it should be noted that the region ahead of the leading shock wave was bright. This suggests that free electrons existed ahead of the leading shock wave and $\partial n_e/\partial x<0$. These free electrons must be produced by bound-free absorption of energetic photons produced in the laser-heated hot plasma.

Figure 6 shows the exposure profiles of the self-emission and Schlieren images. The error bars on the shock-front locations correspond to the accuracy of the timing correlation between the SC and GC. It should be noted that the self emission

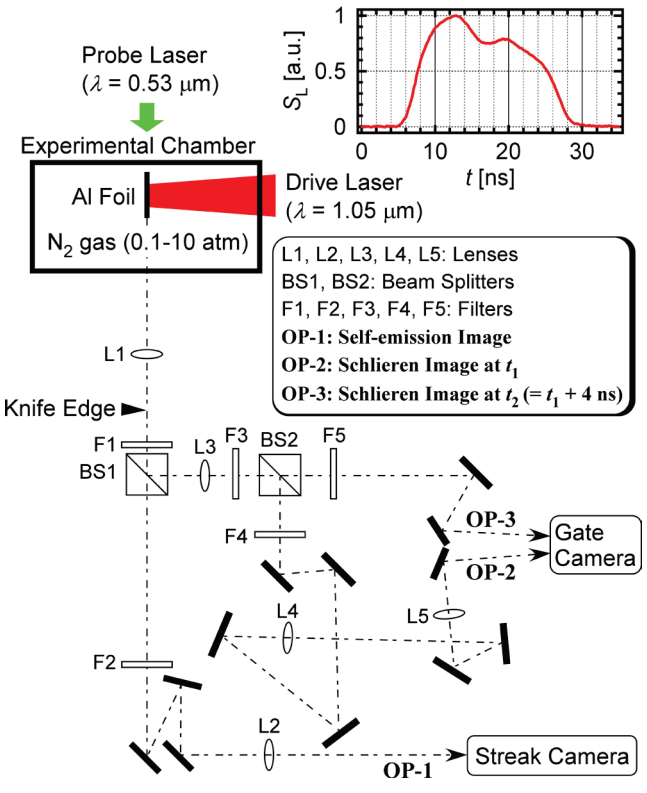

Figure 2. Experimental arrangement.

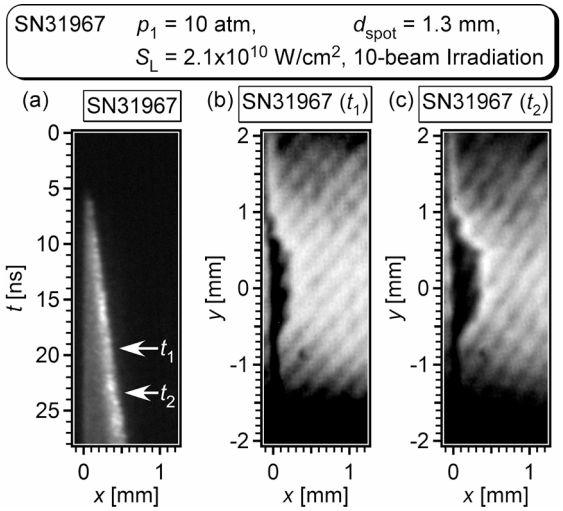

Figure 3. Observed images in a p_1=10 atm case. (a): self-emission image, (b) (c): Schlieren images

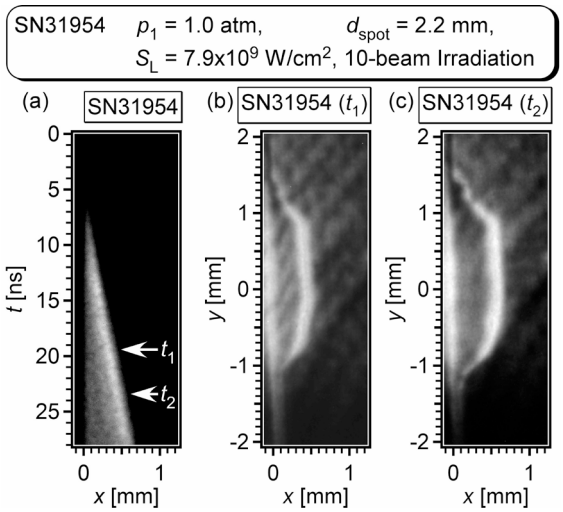

Figure 4. Observed images in a p_1=1.0 atm case. (a): self-emission image, (b) (c): Schlieren images

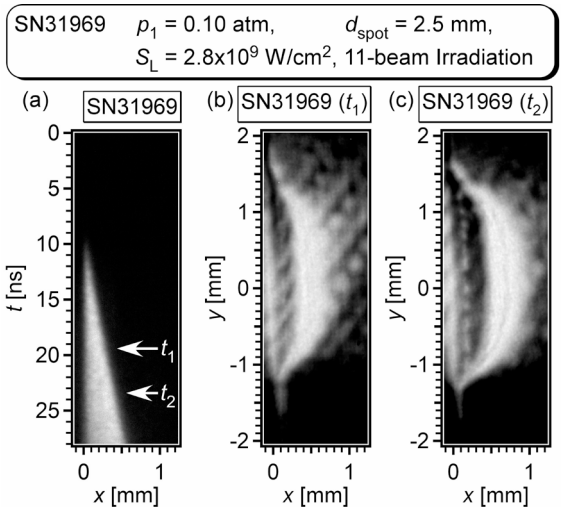

Figure 5. Observed images in a p_1=0.1 atm case. (a): self-emission image, (b) (c): Schlieren images

started earlier than the shock heating. The energetic photons contribute to the heating of the gas ahead of the leading shock wave not only by deposition of their own energy but also by boosting laser absorption. That is, the energetic photons create free electrons, and such free electrons induce laser absorption by inverse bremsstrahlung.

Figure 7 shows detonation speed D obtained from the SC images. Assuming 100% laser absorption, $q_{ext} = S_L/(\rho_1 D_{CJ})$ where ρ_1 is the initial mass density of the gas. Further, assuming $|q_{react}| \propto q_{ext}$, the following scaling law can be obtained from eq. (1).

$$D_{CJ} \propto (S_L/\rho_1)^{1/3} \qquad (3)$$

The data were well described by eq. (3) although they were lower than the calculated D_{CJ}.

All data shown above are of 10 or 11-beam-irradiation cases. On the other hand, in one-beam-irradiation cases, the irradiation uniformity was poor, and corrugated detonations were created. Figure 8 shows such a corrugated front. The propagation distances until t_1 and t_2: $\Delta x(t_1)$ and $\Delta x(t_2)$, at A-G in Fig. 8 are shown in Table 1.

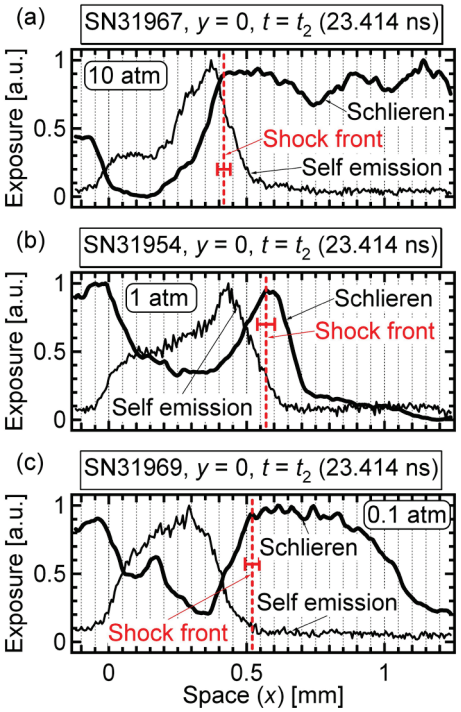

Figure 6. Exposure profiles of self-emission and Schlieren images. (a) p_1=10 atm, (b) p_1=1.0 atm, (c) p_1=0.1 atm.

Assuming that laser energy flux $S_L(y,z,t)$ and detonation speed $D(y,z,t)$ are respectively written as $S_L = \widetilde{S_L}(y,z) f(t)$ and $D \propto S_L(y,z,t)^{1/3}$, the ratio $\Delta x(t_2)/\Delta x(t_1)$ is written as follows.

$$\frac{\Delta x(t_2)}{\Delta x(t_1)} = \frac{\int_0^{t_2} f(t)^{1/3}\,dt}{\int_0^{t_1} f(t)^{1/3}\,dt} \qquad (4)$$

That is, this ratio should be constant. As shown in Table 1, this ratio was almost constant experimentally. The calculated value from the pulse shape in Fig. 2 was 1.67, and agreed well with the experimental results. This means that the corrugated front shown in Fig. 8 was not unstable. This may be due to significant transport effects of energetic photons produced in hot plasma.

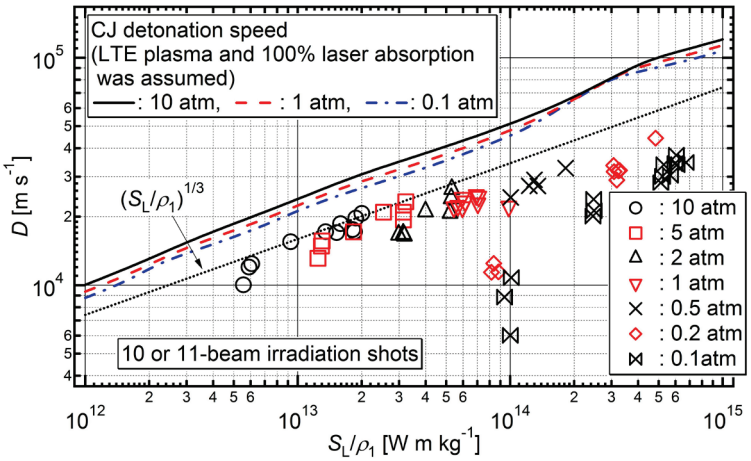

Figure 7. Detonation-propagation speed.

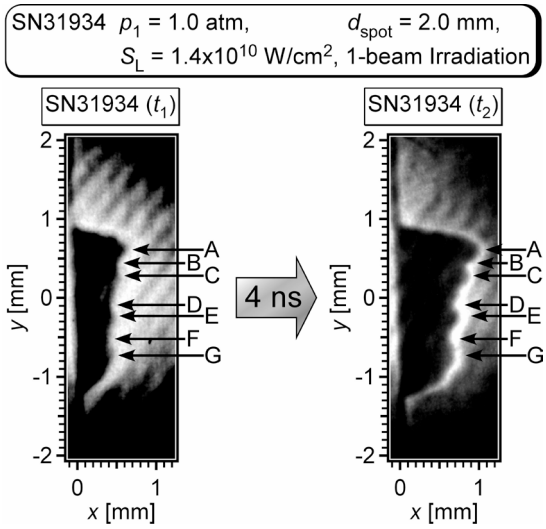

Figure 8. Schlieren images of a corrugated detonation front.

Table 1: Propagation of corrugated front

Position y [mm]	Propagation distance $\Delta x(t_1)$ [mm]	$\Delta x(t_2)$ [mm]	Ratio $\Delta x(t_2)/\Delta x(t_1)$
A (凸): +0.61	0.61	0.97	1.6
B (凹): +0.44	0.49	0.81	1.7
C (凸): +0.28	0.49	0.81	1.7
D (凹): -0.09	0.38	0.64	1.7
E (凸): -0.23	0.42	0.71	1.7
F (凹): -0.52	0.33	0.57	1.7
G (凸): -0.73	0.35	0.60	1.7

4 Conclusions

Quasi-planar laser-driven detonations were generated. It was found that the significant heating of the gas started prior to the shock heating. In nonuniform-irradiation cases, corrugated detonation fronts were created, but they were not unstable.

Acknowledgment

This work was performed as a collaboration research program of the Institute of Laser Engineering, Osaka University.

References

[1] Lee JHS. (2008). The Detonation Phenomenon. Cambridge University Press (ISBN 978-0-521-89723-5).

[2] Ramsden SA, Savic P. (1964). A Radiative Detonation Model for the Development of a Laser-Induced Spark in Air. Nature 203: 1217.

[3] Gauthier P, Chaland F, Masse L. (2004). Deflagration-to-Detonation Transition in Inertial-Confinement-Fusion Baseline Targets. Phys. Rev. E 70: 055401(R).

[4] Timmes FX et al. (2000). On the Cellular Structure of Carbon Detonations. Astrophys. J. 543: 938.

[5] Miyanaga N et al. (2001). The GEKKO XII-HIPER (High Intensity Plasma Experimental Research) System Relevant to Ignition Targets. Proc. 18th Int. Conf. Fusion Energy (IAEA, Sorrento, Italy): IAEA-CN-77.